

Deep Residual Fourier Transformation for Single Image Deblurring

Xintian Mao¹ Yiming Liu¹ Wei Shen² Qingli Li¹ Yan Wang^{1*}

¹ East China Normal University ² Shanghai Jiaotong University

Code: <https://github.com/INVOKERer/DeepRFT>

Abstract

It has been a common practice to adopt the ResBlock, which learns the difference between blurry and sharp image pairs, in end-to-end image deblurring architectures. Reconstructing a sharp image from its blurry counterpart requires changes regarding both low- and high- frequency information. Although conventional ResBlock may have good abilities in capturing the high-frequency components of images, it tends to overlook the low-frequency information. Moreover, ResBlock usually fails to felicitously model the long-distance information which is non-trivial in reconstructing a sharp image from its blurry counterpart. In this paper, we present a Residual Fast Fourier Transform with Convolution Block (Res FFT-Conv Block), capable of capturing both long-term and short-term interactions, while integrating both low- and high-frequency residual information. Res FFT-Conv Block is a conceptually simple yet computationally efficient, and plug-and-play block, leading to remarkable performance gains in different architectures. With Res FFT-Conv Block, we further propose a Deep Residual Fourier Transformation (DeepRFT) framework, based upon MIMO-UNet, achieving state-of-the-art image deblurring performance on GoPro, HIDE, RealBlur and DPDD datasets. Experiments show our DeepRFT can boost image deblurring performance significantly (e.g., with 1.09 dB improvement in PSNR on GoPro dataset compared with MIMO-UNet), and DeepRFT+ even reaches 33.23 dB in PSNR on GoPro dataset.

1. Introduction

Image deblurring aims at removing blurring artifacts to recover sharp images [10]. The blurring/degradation of an image can be caused by many factors, *e.g.*, irregular camera and/or objects movement, out-of-focus optics, etc. The blurry image leads to visually low quality and hampers subsequent high-level vision tasks, ranging from security, medical imaging to object recognition [6].

Substantial research works have been done over the past decades to explore accurate and efficient image de-

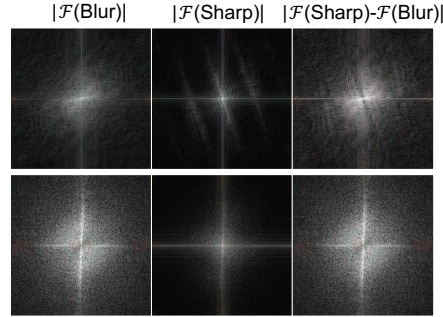


Figure 1. The magnitudes of 2-dimensional discrete Fourier transform (denoted as $|\mathcal{F}(\cdot)|$) of two pairs of blurry vs. sharp images (upper and bottom). The last column shows the absolute value of the magnitude subtraction. The difference in frequency domain lies in both low and high frequency (see the right-most column).

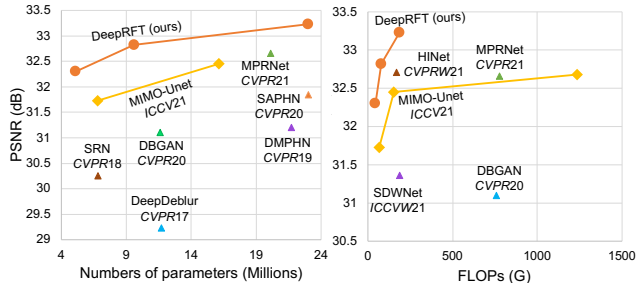


Figure 2. Image deblurring on the GoPro dataset [27]. PSNR vs. number of parameters and PSNR vs. FLOPs. Our method performs much better than the baseline method MIMO-UNet [10] and state-of-the-arts.

blurring approaches. But, due to the ill-posed nature of the subject, image deblurring is still an unsolved problem. Kernel-based methods try to estimate the latent sharp image and the blur operator simultaneously, given a blurry image [4, 32, 36, 40, 43]. But kernel-related problems usually hamper its usage in effective image deblurring, *e.g.*, kernel estimation is sensitive to noise, and there often exist various constraints to model characteristics of blur which are not practical in real scenarios.

DeepDeblur [27], pioneers the technique of end-to-end trainable methods, directly mapping a blurry image to its

*Corresponding author: Y. Wang (ywang@cee.ecnu.edu.cn)

paired sharp image by a Convolutional Neural Network (CNN). It designs a multi-scale architecture, and uses a modified residual network structure [14] called ResBlock to focus on learning the difference between blurry and sharp image pairs. Thereafter, ResBlock is proven to be effective in image deblurring, and becomes a widely accepted module in various end-to-end image deblurring architectures [5, 10, 29, 42, 49, 51, 56]. Though these methods have furthered the efficacy compared with most kernel-based methods, there are still severe limitations yet to be tackled: (1) ResBlock is commonly instantiated by CNNs, whose effective receptive field size is limited, especially in early layers. Thereon, ResBlock techniques proposed in literature corpus usually fail to felicitously model the global information which is non-trivial in learning discrepancy between blurry and sharp image pairs, *e.g.*, the context for understanding the global structure of the blur. (2) These methods rarely delicately design the ResBlock tailored to capture the true discrepancy between blurry and sharp image pairs from the perspective of frequency domain, which should be paid more attention to for image deblurring. Concretely, we notice that compared with the blurry image, the sharp image contains much less low-frequency information [†] and more high-frequency information, (see Fig. 1). As is known, CNNs are prone to capture elementary visual features from edges or contours, especially in lower layers, while the higher layers tend to combine these features [50]. As also suggested by a more recent work [44], we conclude that ResBlock may be armed with good abilities in learning high-frequency components, and might lack a powerful representation ability in modeling low-frequency information.

To alleviate the problems mentioned above, in this work, we propose a Residual Fast Fourier Transform with Convolution Block (Res FFT-Conv Block), a conceptually simple, effective and plug-and-play block, leading to remarkable performance gains in different image deblurring architectures. The Res FFT-Conv Block contains two streams for residual learning: (1) The FFT-Conv stream uses a 1×1 convolution after converting the spatial feature map to the frequency domain, enabling both the low and high frequency learning. Due to the properties of FFT, it also allows the image-wide receptive field that covers the entire image starting from early layers. It captures the global discrepancy between blurry and sharp image pairs effortlessly, which is crucial for high resolution image deblurring. (2) The normal convolution stream focuses on the local details and prone to learn high-frequency differences.

We further present a Deep Residual Fourier Transformation (DeepRFT) framework, by plugging our Res FFT-Conv Block into MIMO-UNet [10]. MIMO-UNet is one of the most recent ResBlock-based models with

[†]Compared with sharp image, the low-frequency information in blurry image can be generated by situations such as severe motion.

remarkable speed advantages among existing networks. In order to achieve noticeable deblurring performance improvement compared with state-of-the-arts, we additionally replace convolution operation by Depthwise Over-parameterized Convolution (DO-Conv) [3] in DeepRFT. Over-parameterization has been proven as a way to accelerate the training of deep networks. We show that DO-Conv can introduce some performance gains for image deblurring without incurring extra parameters for inference.

The effectiveness of Res FFT-Conv Block is compared and verified by plugging in different architectures. We also verify our proposed DeepRFT on GoPro [27], HIDE [37] RealBlur [33], and DPDD [1] datasets. Without bells and whistles, DeepRFT achieves 32.82 dB in terms of PSNR on GoPro datasets, with 1.09 dB improvement compared with MIMO-UNet, and DeepRFT+ reaches 33.23 dB. Our method noticeably improves MIMO-UNet without introducing too many parameters, while maintaining a low computational complexity. The PSNR vs. Params (M) and PSNR vs. FLOPs (G) compared with state-of-the-art methods are shown in Fig. 2.

2. Related Work

2.1. Deep Image Deblurring

Deep learning methods have achieved significant success in image deblurring [10, 19, 20, 27, 40, 42, 49, 56] as well as other low-level vision tasks such as image denoise [7, 48], image deraining [16] and image super-resolution [11, 13, 26, 54]. Sun *et al.* [40] propose to estimate the spatially-varying kernels of motion blur by a CNN. But, since the characteristics of blur are complex, the blur kernel estimation method is not practical in real scenarios. Later, DeepDeblur [27], without estimating the blur kernel, directly maps a blurry image to its sharp counterpart. Scale-recurrent network [42] proposes an encoder-decoder structure to yield training feasibility. Adversarial training has also been extensively studied [19, 20]. Most of these networks perform CNNs on the spatial domain to recover the sharp image from its blurry image. But, after MPRNet [49], performances of methods based upon the spatial domain fall into the bottleneck. The performance of MPRNet on GoPro dataset [27] is hard to be surpassed. To address this problem, we propose to learn the knowledge from both the spatial and the frequency domain, which is able to achieve 0.57 dB improvement in PSNR with much less FLOPs and runtime compared with MPRNet.

Transformer/non-local has strong global context modeling ability and has shown its great promise in various computer vision tasks. A few transformer-based image restoration methods have been proposed, such as SwinIR [23]. But its considerable computational complexity usually hampers its usage in efficient image restoration. We test the model

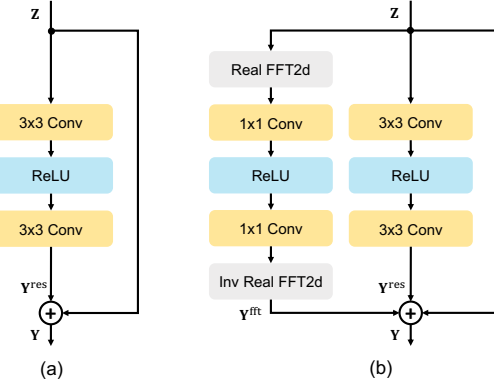


Figure 3. (a) ResBlock. (b) Proposed Res FFT-Conv Block.

of SwinIR [23] on GoPro dataset, which takes 1.99s per image, even two times slower than MPRNet.

2.2. End-to-end Deblur Model with ResBlock

DeepDeblur [27] designs a residual block (ResBlock) based on Conv-ReLU-Conv structure. Thereafter, ResBlock has become one fundamental block in image deblurring [10, 29, 42, 51]. Various efforts have been devoted to modifying the ResBlock, *e.g.*, the content-aware processing module proposed by SAPHN [39], the channel attention block proposed by MPRNet [49], the HIN block proposed by HINet [5], and the dilated conv block proposed by SD-WNet [56]. All mentioned methods focus on extracting information from the spatial domain, and overlook important discrepancies in the frequency domain. We propose a Res FFT-Conv Block from the perspective of image’s frequency, capturing both high- and low- frequency discrepancies.

2.3. Applications of Fourier Transform

In recent years, some methods extracted information from the frequency domain to fulfill different tasks are proposed [9, 31, 34, 41, 46, 55]. FDA [46] swaps the low-frequency spectrum between images to mitigate the influence caused by the images’ style change for image segmentation. GFNet [31] learns long-term spatial dependencies in the frequency domain for image classification. LaMa [41] applies the structure of fast Fourier convolution [8] to image inpainting. In image deblurring, SDWNet [56] introduces wavelet transform into deep networks. Inspired by the success of Fast Fourier Transform (FFT), we propose a Res FFT-Conv Block which can effectively model the frequency information to deblur an image.

3. Methodology

3.1. ResBlock

Before introducing our proposed method, we first revisit the residual building block in image deblurring tasks, which

is called ResBlock. Specifically, ResBlock consists of two 3×3 convolutional layers and one ReLU layer in between, as shown in Fig. 3 (a). ResBlock enables deeper architecture, larger receptive field size, and fast convergence speed at training time.

The success of ResBlock suggests that properly learning the difference of blurry and sharp image pairs improves model performance. As discussed in Sec. 1 and Fig. 1, both the high-frequency and low-frequency discrepancy should be modeled in ResBlock. A convolutional operator has good abilities in learning high-frequency details, as it usually captures informative features from edges. Thus, it may lack a powerful representation ability in modeling low-frequency information. Moreover, to reconstruct a high quality sharp image from its blurry counterpart, the ability of understanding the content globally is non-trivial. Though the effective receptive field size can be enlarged by stacking more ResBlocks, a big receptive field size in the early layer is still missing, and the computation complexity can be largely increased by stacking. In addition, techniques which capture long-range dependencies such as non-local has been explored in low level vision tasks [26], the efforts to reduce high memory requirements may lead to sub-optimal solutions, as discussed in [39].

3.2. Residual Fast Fourier Transform Block

We propose a Residual Fast Fourier Transform with Convolution Block (Res FFT-Conv Block) to replace the ResBlock. Such building block enjoys benefits from modeling both high-frequency and low-frequency discrepancies between blurry image and sharp image pairs, while capturing both long-term and short-term interactions. As shown in Fig. 3 (b), besides a normal spatial residual stream, we simply add another stream based on a channel-wise FFT [2] to account for the global context in the frequency domain. Discrete Fourier Transform (DFT) is widely used in modern signal processing algorithms, whose 1D version can be derived by:

$$X[k] = \sum_{n=0}^{N-1} x[n] e^{-j \frac{2\pi}{N} kn}, \quad (1)$$

where $x[n]$ is a sequence of N complex numbers, $X[k]$ indicates the spectrum at the frequency $\omega_k = 2\pi k/N$, and j represent the imaginary unit. It is clear that the spectrum at any frequency has global information. Noted that the DFT of a real signal $x[n]$ is *conjugate symmetric*, *i.e.*,

$$X[N-k] = \sum_{n=0}^{N-1} x[n] e^{-j \frac{2\pi}{N} (N-k)n} = X^*[k]. \quad (2)$$

The same applies to 2D DFT, which performs sequential row and column 1D DFT on a 2D signal whose size is $M \times N$, *i.e.*, $X[M-u, N-v] = X^*[u, v]$. Since the results of a real array’s DFT has symmetric properties, the

right half of the results can be derived from the left half. The FFT algorithms reduce the complexity and calculates the DFT in a more efficient way. Let $\mathbf{Z} \in \mathbb{R}^{H \times W \times C}$ be the input feature volume, where H , W , and C indicate the height, width and channel of the feature volume. The left most stream in Res FFT-Conv Block (see Fig. 3 (b)) is processed as follows:

- (1) computes 2D real FFT of \mathbf{Z} and obtain $\mathcal{F}(\mathbf{Z}) \in \mathbb{C}^{H \times W/2 \times C}$;
- (2) concatenates the real part $\mathcal{R}(\mathcal{F}(\mathbf{Z}))$ and the imaginary part $\mathcal{I}(\mathcal{F}(\mathbf{Z}))$ along the channel dimension to acquire $\tilde{\mathbf{Z}} = \mathcal{R}(\mathcal{F}(\mathbf{Z})) \odot_C \mathcal{I}(\mathcal{F}(\mathbf{Z})) \in \mathbb{R}^{H \times W/2 \times 2C}$, where \odot_C represents concatenation through the channel dimension;
- (3) uses two stacks of 1×1 convolution layers (convolution operator $*$) with a ReLU layer in between: $f(\tilde{\mathbf{Z}}; \Theta^{(1)}, \Theta^{(2)}) = \text{ReLU}(\tilde{\mathbf{Z}} * \Theta^{(1)}) * \Theta^{(2)} \in \mathbb{R}^{H \times W/2 \times 2C}$, and $f(\tilde{\mathbf{Z}}; \Theta^{(1)}, \Theta^{(2)})$ will be termed as f for simplicity;
- (4) applies inverse 2D real FFT to transform $f = f^{\text{real}} \odot_C f^{\text{img}}$ back to spatial domain: $\mathbf{Y}^{\text{fft}} = \mathcal{F}^{-1}(f^{\text{real}} + j f^{\text{img}}) \in \mathbb{R}^{H \times W \times C}$, where $f^{\text{real}}, f^{\text{img}} \in \mathbb{R}^{H \times W/2 \times C}$.

Here, all frequencies share the identical convolution kernel, enabling the modeling of all frequencies' information and correlations. Then the final output of Res FFT-Conv Block is calculated via $\mathbf{Y} = \mathbf{Y}^{\text{fft}} + \mathbf{Y}^{\text{res}} + \mathbf{Z}$, where \mathbf{Y}^{res} uses the same computation as that in the original ResBlock.

3.3. Deep Residual Fourier Transform Framework

Our Deep Residual Fourier Transformation (DeepRFT) framework is designed based upon MIMO-UNet [10], a multi-input multi-output U-Net [35] architecture for efficient multi-scale image deblurring. The overall framework of our DeepRFT is depicted in Fig. 4. We replace all Res-Blocks in MIMO-UNet by our Res FFT-Conv Blocks. In order to achieve noticeable deblurring performance gains compared with all state-of-the-art methods, we additionally replace convolution operation by DO-Conv [3].

Depthwise over-parameterized convolution DO-Conv has shown its potential in many high-level vision tasks such as image classification, semantic segmentation and object detection [3]. DO-Conv speeds up the training with more parameters and achieves better performance by augmenting a convolutional layer with a depthwise convolution. We will show in the experiment that adding DO-Conv to image deblurring can help converge to a slightly lower loss. Meanwhile, DO-Conv is two adjacent linear operations, which can be combined into a traditional convolution operation during inference time. Inspired by this, we replace all non 1×1 convolutions with DO-Conv.

Loss Function Let $k \in \{0, \dots, K-1\}$, $\hat{\mathbf{S}}_k$, \mathbf{S}_k and ε denote the k th level in DeepRFT, the k th reconstructed image, the k th groundtruth sharp image, and a constant value 10^{-3} , respectively. In order to train DeepRFT, three kinds of loss functions are adopted:

- (1) Multi-Scale Charbonnier (MSC) loss [49]:

$$\mathcal{L}_{msc} = \sum_{k=0}^{K-1} \sqrt{\|\hat{\mathbf{S}}_k - \mathbf{S}_k\|^2 + \varepsilon^2}. \quad (3)$$

- (2) Multi-Scale Edge (MSED) loss [49]:

$$\mathcal{L}_{msed} = \sum_{k=0}^{K-1} \sqrt{\|\Delta(\hat{\mathbf{S}}_k) - \Delta(\mathbf{S}_k)\|^2 + \varepsilon^2}, \quad (4)$$

where Δ denotes the Laplacian operator.

- (3) Multi-Scale Frequency Reconstruction (MSFR) loss [10], which evaluates the difference of the multi-scale reconstructed images and the groundtruth sharp images in the frequency domain:

$$\mathcal{L}_{msfr} = \sum_{k=0}^{K-1} \|\mathcal{FT}(\hat{\mathbf{S}}_k) - \mathcal{FT}(\mathbf{S})\|_1, \quad (5)$$

where \mathcal{FT} represents the FFT operation. Finally, the loss function for DeepRFT is: $\mathcal{L} = \mathcal{L}_{msc} + \alpha_1 \mathcal{L}_{msed} + \alpha_2 \mathcal{L}_{msfr}$, where α_1 and α_2 are tradeoff-parameters and are empirically set to 0.05 as in [49] and 0.01, respectively.

4. Experiments

4.1. Dataset and Implementation Details

In this section, we evaluate DeepRFT on four datasets: GoPro [27], HIDE [37], RealBlur [33] and DPDD [1] datasets. Since existing methods adopt different experimental settings, we summarize them and report four groups of results: (I) train on 2,103 pairs of blurry and sharp images in GoPro dataset, and test on 1,111 image pairs in GoPro (follow [10]), 2,025 image pairs in HIDE (follow [49]), 980 image pairs in RealBlur-R test set, and 980 image pairs in RealBlur-J test set (follow [49]), respectively; (II) train on 3,758 image pairs in RealBlur-R, and test on 980 image pairs in RealBlur-R (follow [49]), and train on 3,758 image pairs in RealBlur-J, and test on 980 image pairs in RealBlur-J (follow [49]); (III) train on GoPro and RealBlur-J training sets, and test on RealBlur-J test set [10] to compare with the results reported in MIMO-UNet [10]; (IV) train and test on the defocus deblurring dataset: DPDD [1], where 500 dual-pixel images are split into training, validation, and testing sets, each of which contains 350, 74 and 76 scenes (follow [22]).

We adopt the training strategy used in MPRNet [49] unless otherwise specified. *I.e.*, the network training hyper-parameters (and the default values we use) are patch size (256 \times 256), batch size (16), training epoch (3,000), optimizer (Adam [18]), initial learning rate (2×10^{-4}). The

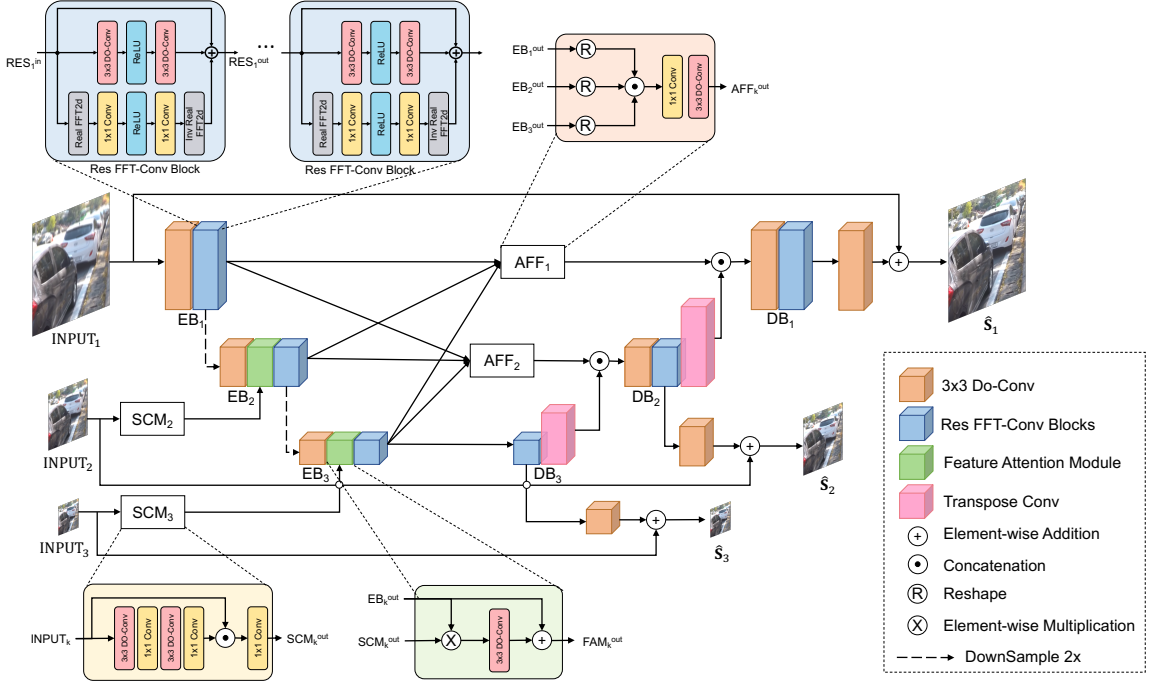


Figure 4. The framework of DeepRFT. DeepRFT is designed based upon MIMO-UNet [10], which takes multi-scale input blurry images and generates multi-scale output sharp images. The ResBlocks are replaced by Res FFT-Conv Blocks. Non 1×1 convolutional layers are replaced by DO-Conv. AFF, SCM, EB and DB are short for asymmetric feature fusion, shallow convolutional module, encoder block and decoder block, respectively.

learning rate is steadily decreased to 1×10^{-6} using the cosine annealing strategy [25]. Following [49], horizontal and vertical flips are randomly applied on patches for data augmentation. For testing, we adopt the same dataset slicing crop method as used in SDWNet [56], where we utilize a step of 256 to perform 256×256 size sliding window slicing, and compensate slicing on the edge part (for the overlap part, we directly use the non-edge patch).

4.2. Experimental Results

Evaluation metric:

The average performance of PSNR and SSIM over all testing sets are computed and compared by using the official software released by [49] unless otherwise specified. We also report number of parameters, FLOPs, and testing time per image on a workstation with Intel Xeon Gold 6240C CPU, NVIDIA GeForce RTX 3090 GPU.

Evaluation of Res FFT-Conv Block:

Our Res FFT-Conv Block is a plug-and-play block. In order to show its effectiveness in improving image deblurring performance in various architectures, we plug it into U-Net and ORSNet (two backbone networks used in MPRNet [49]); MPRNet-small [49], whose number of channels is three times smaller than original MPRNet due to limited computation resource; and MIMO-UNet [10]. For U-Net, ORSNet and MPRNet-small, we train 1000 epochs with

Table 1. Evaluation of Res FFT-Conv Block on GoPro [27] and HIDE [37] (Group I setting). FFT indicates whether the ResBlock in the original architecture is replaced by our Res FFT-Conv Block. \times means the results are obtained by the original architecture. All models are trained by ourselves for fair comparison.

Model	FFT	GoPro [27]		HIDE [37]	
		PSNR	SSIM	PSNR	SSIM
U-Net [49]	\times	29.87	0.930	28.45	0.906
	✓	31.13	0.946	29.51	0.924
ORSNet [49]	\times	29.34	0.924	28.07	0.899
	✓	31.77	0.953	30.10	0.930
MPRNet-small [49]	\times	29.97	0.932	28.68	0.910
	✓	31.75	0.952	30.27	0.933
MIMO-UNet [10]	\times	31.92	0.953	29.65	0.925
	✓	32.74	0.960	30.90	0.939

a patch size of 256. The loss function is a combination of Charbonnier loss and Edge loss, followed by [49]. For MIMO-UNet, we use the same training strategy as illustrated in Sec. 4.1, with a combination of MSC loss, MSED loss and MSFR loss as the loss function. PSNR/SSIM on GoPro and HIDE datasets in Group I setting are summarized in Table 1. Replacing ResBlock by our Res FFT-Conv Block leads to remarkable performance gains in various architectures. *E.g.*, for ORSNet, *w/ Res FFT-Conv Block* outperforms *w/ ResBlock* by 2.43 dB in PSNR on the GoPro dataset.

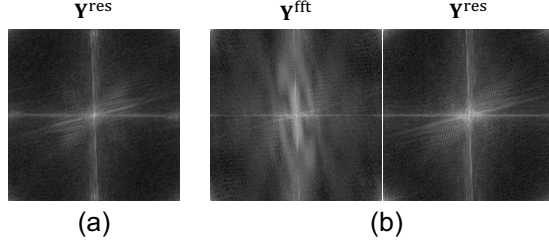


Figure 5. Average magnitudes of 2D FFT of learned last residual features in well-trained models on GoPro dataset [27]. (a) ResBlock in MIMO-UNet and (b) Res FFT-Conv Block in *MIMO-UNet w/ Res FFT-Conv Block* model, respectively.

Next, we show Res FFT-Conv Block captures more low-frequency discrepancy than ResBlock. We visualize the average magnitudes of 2D FFT of the residual features in Fig. 5. The features are extracted from the last ResBlock in the well-trained MIMO-UNet (Fig. 5(a)), and the last Res FFT-Conv Block in the well-trained *MIMO-UNet w/ Res FFT-Conv Block* model (Fig. 5(b)) on GoPro dataset [27]. \mathbf{Y}^{fft} learns much more low-frequency information than \mathbf{Y}^{res} . It is also interesting to observe that the learned \mathbf{Y}^{res} in *MIMO-UNet w/ Res FFT-Conv Block* is armed with more low-frequency information than \mathbf{Y}^{res} in MIMO-UNet. The reason may be that the former \mathbf{Y}^{res} contains low-frequency information learned via Res FFT-Conv Blocks in lower layers.

Evaluation of DeepRFT:

We compare our DeepRFT with state-of-the-art methods. MIMO-UNet has three variants, *i.e.*, MIMO-UNet (8 residual blocks for each EB and DB), MIMO-UNet+ (20 residual blocks for each EB and DB), and MIMO-UNet++ (estimate MIMO-UNet+ with the geometric self-ensemble method [24]). Since we cannot access the specific augmentations which are exploited in MIMO-UNet++, we only design DeepRFT based upon the first two variants, acquiring DeepRFT and DeepRFT+. Besides, we reduce the number of Res FFT-Conv block to 4 for each EB and DB, and obtain an extra model termed as DeepRFT-small.

PSNR, SSIM and number of parameters in inference on GoPro and HIDE datasets of Group I setting are shown in Table 2. Our DeepRFT-small outperforms MIMO-UNet by 0.57 dB PSNR with 1.7M less parameters. DeepRFT+ achieves the best performance, and even outperforms an eight-time assembled model MIMO-UNet++ with a clear margin (0.55 dB PSNR). For a fair comparison with SD-WNet [56], we use the same PSNR/SSIM computation codes released by [56], and report the results in Table 3.

Following the experimental setting used in [49], we directly test the model (trained on GoPro dataset) on RealBlur-R and RealBlur-J datasets (Group I setting). The quantitative comparisons on RealBlur datasets are shown in top regions in Table 4. DeepRFT and DeepRFT+ achieve

Table 2. Performance comparison on GoPro [27] and HIDE [37] (Group I setting). The best and 2nd best results are **highlighted** and underlined. \ddagger means testing an image for 8 times by test time augmentation. $*$ denotes results tested by using released models.

Model	GoPro [27]		HIDE [37]		Params (M)
	PSNR	SSIM	PSNR	SSIM	
DeepDeblur [27]	29.23	0.916	N/A	N/A	11.7
SRN [42]	30.26	0.934	28.36	0.915	6.8
DeblurGAN [19]	28.70	0.858	24.51	0.871	N/A
DeblurGAN-v2 [20]	29.55	0.934	26.61	0.875	60.9
PSS-NSC [12]	30.92	0.942	N/A	N/A	2.84
DMPHN [51]	31.20	0.945	29.09	0.924	21.7
SAPHN [39]	31.85	0.948	29.98	0.930	23.0
MT-RNN [29]	31.15	0.945	29.15	0.918	2.6
RADN [30]	31.76	0.953	N/A	N/A	N/A
SVDN [47]	29.81	0.937	N/A	N/A	N/A
DBGAN [53]	31.10	0.942	28.94	0.915	11.6
MPRNet [49]	32.66	0.959	30.96	0.939	20.1
MIMO-UNet [10]	31.73	0.951	29.28 [*]	0.921 [*]	6.8
MIMO-UNet+ [10]	32.45	0.957	29.99 [*]	0.930 [*]	16.1
MIMO-UNet++ [10]	32.68	0.959	N/A	N/A	16.1 \ddagger
HINet [5]	32.71	0.959	N/A	N/A	88.7
DeepRFT-small	32.30	0.956	30.42	0.934	5.1
DeepRFT	<u>32.82</u>	<u>0.960</u>	<u>30.99</u>	<u>0.941</u>	9.6
DeepRFT+	33.23	0.963	31.42	0.944	23.0

Table 3. Performance comparison with SDWNet [56] (Group I setting). We obtain slightly different PSNRs/SSIMs on DeepRFT by using the PSNR/SSIM computation codes released by [56].

Model	GoPro [27]		HIDE [37]		Params (M)
	PSNR	SSIM	PSNR	SSIM	
SDWNet [56]	31.36	0.967	29.23	0.963	7.2/189.7
DeepRFT-small	32.48	0.973	30.54	0.966	5.1/44.6
DeepRFT	33.00	0.975	31.11	0.969	9.6/80.2
DeepRFT+	33.42	0.977	31.55	0.970	23.0/187.0

the state-of-the-art results on two datasets with 36.06 dB PSNR and 28.97 dB PSNR, respectively. MPRNet [49] yields the 2nd best result in RealBlur-R dataset. It is worth mentioning that the FLOPs number of MPRNet is 777.01G, which is much larger than ours (80.21G for DeepRFT and 187.04G for DeepRFT+, see Table 6).

We also train and test on RealBlur dataset [49] (Group II setting). Results are compared in Table 4 with symbol \ddagger . 0.53 dB and 0.43 dB PSNR performance gains are achieved on RealBlur-R and RealBlur-J compared with MPRNet.

Besides, to compare with MIMO-UNet [10] who uses the GoPro and RealBlur-J training datasets for training models and RealBlur-J test datasets for testing, we conduct experiments following the Group III setting. Detailed comparisons are illustrated in the bottom region in Table 4 with symbol \ddagger . Our DeepRFT+ achieves improvement of 0.23 dB PSNR compared with MIMO-UNet++.

To show the effectiveness of DeepRFT in single image defocus deblurring, we train and test our model on the

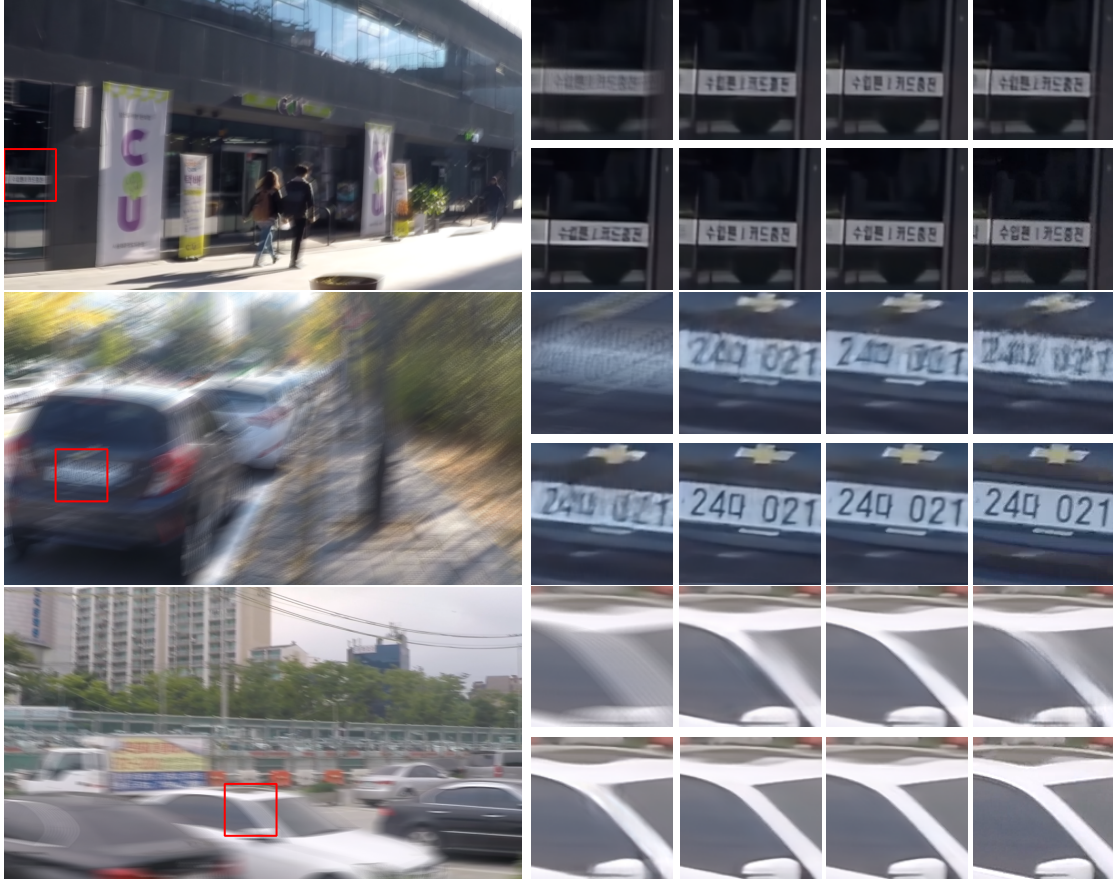


Figure 6. Examples on the GoPro test dataset. The original blur image and the zoom-in patches are shown. From left-top to right-bottom are Blurry image, results obtained through DMPHN, MIMO+, HINet, MPRNet, DeepRFT, DeepRFT+, and the Groundtruth sharp image.

DPDD dataset. Results computed using the codes released by IFAN [22] are shown in Table 5. Our DeepRFT surpasses all state-of-the-arts in PSNR, SSIM and MAE with less number of parameters. DeepRFT achieves comparable LPIPS compared with IFAN [22]. It is worth mentioning that IFAN is specifically designed for dealing with defocus deblur, and uses dual-pixel stereo images for training. We only use blur images.

Some of the predicted sharp images from the GoPro dataset are shown in Fig. 6. Results from competitors are tested by using their released models. DeepRFT is more successful in deblurring local details and structures compared with others.

FLOPs and runtime comparison:

We compare FLOPs and runtime with the state-of-the-arts (see Table 6). FLOPs number is calculated using pt-flops[‡] with the input size of 256×256 [56]. Runtime is measured by using the released test code of each method to run the entire GoPro [27] testing dataset, and obtaining the average runtime (second) per image on our environment

with a single NVidia 3090 GPU. Our DeepRFT+ is about 3 times faster than MIMO-UNet++ and about 2 times faster than MPRNet, while achieving 0.55 dB and 0.57 dB improvements in terms of PSNR, respectively.

Ablation study and discussion:

We conduct ablation experiments on the GoPro dataset [27] to show the effectiveness of each module in DeepRFT. As shown in Table 7, Res FFT-Conv Block significantly boosts PSNR by 0.74 dB. Replacing convolutional layers by DO-Conv further improves the results by 0.08 dB, without introducing more parameters or runtime in inference. Using only the FFT stream in Res FFT-Conv Block leads to performance drop (see \checkmark^{**} in Table 7). We also try to replace Res FFT-Conv Block by a recently developed *fast Fourier convolutions* [8] operator which has shown its potential in image inpainting [41], but it does not help in improving image deblurring performance.

Fig. 7 shows training curves corresponding to the first (*i.e.*, MIMO), second and fourth row in the result part of Table 7. Res FFT-Conv Block and DO-Conv converge faster and to lower losses, especially the Res FFT-Conv Block.

[‡]<https://github.com/sovrasov/flops-counter.pytorch>

Table 4. Performance comparison on RealBlur datasets [33] (Group I, II, III settings). Group II and Group III results are with \P and \S , respectively. DeepRFT, DeepRFT+ are proposed based on MIMO-UNet and MIMO-UNet+, respectively. DeepRFT-small reduces the number of Res FFT-Conv Block to 4. * denotes the results tested by using released models.

Model	RealBlur-R		RealBlur-J	
	PSNR	SSIM	PSNR	SSIM
Hu <i>et al.</i> [15]	33.67	0.916	26.41	0.803
DeepDeblur [27]	32.51	0.841	27.87	0.827
DeblurGAN [19]	33.79	0.903	27.97	0.834
Pan <i>et al.</i> [28]	34.01	0.916	27.22	0.790
Xu <i>et al.</i> [45]	34.46	0.937	27.14	0.830
DeblurGan-v2 [20]	35.26	0.944	28.70	0.866
Zhang <i>et al.</i> [52]	35.48	0.947	27.80	0.847
SRN [42]	35.66	0.947	28.56	0.867
DMPHN [51]	35.70	0.948	28.42	0.860
MPRNet [49]	35.99	0.952	28.70	0.873
MIMO-UNet [10]	35.47*	0.946*	27.76*	0.836*
MIMO-UNet+ [10]	35.54*	0.947*	27.63*	0.837*
DeepRFT-small	35.89	0.952	28.60	0.868
DeepRFT	36.06	0.954	28.90	0.880
DeepRFT+	35.86	0.950	28.97	0.884
DeblurGan-v2 \P [20]	36.44	0.935	29.69	0.870
SRN \P [42]	38.65	0.965	31.38	0.909
MPRNet \P [49]	39.31	0.972	31.76	0.922
DeepRFT+ \P	39.84	0.972	32.19	0.931
MIMO-UNet+ \S [10]	N/A	N/A	31.92	0.919
MIMO-UNet++ \S [10]	N/A	N/A	<u>32.05</u>	0.921
DeepRFT+ \S	N/A	N/A	32.28	0.929

Table 5. Performance comparison on the DPDD dataset [1] (Group IV setting). DeepRFT surpasses all other methods in PSNR, SSIM and MAE. It achieves comparable LPIPS with IFAN [22], which is specifically designed for image defocus deblurring.

Model	PSNR \uparrow	SSIM \uparrow	MAE $(\times 10^{-1}) \downarrow$	LPIPS \downarrow	Params (M)
Input	23.89	0.725	0.471	0.349	N/A
JNB [38]	23.69	0.707	0.480	0.442	N/A
EBDB [17]	23.94	0.723	0.468	0.402	N/A
DMENet [21]	23.90	0.720	0.470	0.410	26.94
DPDNet _S [1]	24.03	0.735	0.461	0.279	35.25
DPDNet _D [1]	25.23	0.787	0.401	0.224	35.25
IFAN [22]	<u>25.37</u>	<u>0.789</u>	<u>0.394</u>	0.217	10.48
DeepRFT	25.71	0.801	0.389	0.218	9.6

5. Conclusion

In this paper, we present Deep Residual Fourier Transformation (DeepRFT) for image deblurring, where we propose a plug-and-play residual block called Res FFT-Conv Block, integrating both spatial and frequency residual information. Res FFT-Conv Block allows the image-wide receptive field which is able to capture the long-term interaction. By plugging Res FFT-Conv Block into MIMO-UNet, our DeepRFT achieves remarkable superior performance compared with all state-of-the-arts. Experiments are evaluated on four image deblurring datasets.

Table 6. FLOPs and runtime comparison. PSNR is shown as a reference. Runtime shows the average testing time per image in GoPro [27] dataset on a single NVidia 3090 GPU. PSNR calculated using codes released by [56] are shown with \dagger , whose details are illustrated in Table 3.

Model	PSNR	FLOPs (G)	Runtime (s)
DMPHN [51]	31.20	N/A	0.307
DBGAN [53]	31.10	759.85	1.298
MPRNet [49]	32.66	777.01	1.002
MIMO-UNet [10]	31.37	67.17	0.153
MIMO-UNet+ [10]	32.45	154.41	0.309
MIMO-UNet++ [10]	32.68	1235.26	2.467
SDWNet [56]	31.36 \dagger	189.68	0.533
DeepRFT-small	32.30	44.60	0.204
DeepRFT	<u>32.82</u>	80.21	0.345
DeepRFT+	33.23	187.04	0.786

Table 7. Ablation on GoPro dataset [27]. MIMO indicates original MIMO-UNet [10], but trained with our strategy (Sec. 4.1) and loss functions (Eq. 3 - 5); FFT indicates Res FFT-Conv Block; DC denotes DO-Conv [3]. \checkmark ** indicates removing the middle stream in Res FFT-Conv Block (Fig. 3 (b)). FFC denotes replacing Res FFT-Conv Block in DeepRFT by *fast Fourier convolutions* [41].

MIMO	FFT	DC	PSNR	Params (M)	Runtime (s)	FLOPs (G)
\checkmark			31.92	6.8	0.134	67.03
\checkmark	\checkmark		32.74	9.6	0.345	80.21
\checkmark		\checkmark	32.18	6.8	0.134	67.03
\checkmark	\checkmark	\checkmark	32.82	9.6	0.345	80.21
\checkmark	\checkmark **	\checkmark	31.00	3.4	0.235	22.17
\checkmark	FFC	\checkmark	31.11	7.7	0.508	72.10

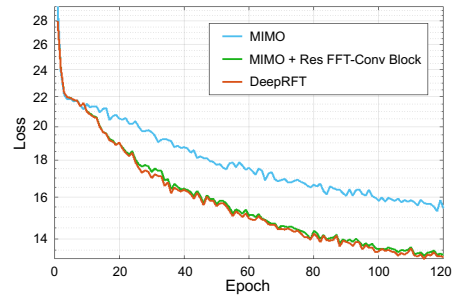


Figure 7. Training loss curves. 120 epochs are shown.

DeepRFT+ \S [10]

Limitations and broader impacts. The proposed method has accomplished a primary exploration of the frequency domain. The Res FFT-Conv Block introduces slightly more parameters than ResBlock. A great many studies are worth exploring by following our work, to acquire even faster speed and better performance. Besides, the proposed model may generate details used to pry into other people's privacy. Thus, the model should be used in a right way.

References

- [1] Abdullah Abuolaim and Michael S. Brown. Defocus deblurring using dual-pixel data. In *ECCV*.
- [2] E. O. Brigham and R. E. Morrow. The fast fourier transform. *IEEE Spectrum*, 4(12):63–70, 1967.
- [3] Jinning Cao, Yangyan Li, Mingchao Sun, Ying Chen, Dani Lischinski, Daniel Cohen-Or, Baoquan Chen, and Changhe Tu. Do-conv: Depthwise over-parameterized convolutional layer. *CoRR*, abs/2006.12030, 2020.
- [4] Ayan Chakrabarti. A neural approach to blind motion deblurring. In *ECCV*, 2016.
- [5] Liangyu Chen, Xin Lu, Jie Zhang, Xiaojie Chu, and Cheng-peng Chen. Hinet: Half instance normalization network for image restoration. In *CVPR Workshop*, 2021.
- [6] Xu Chen, James J. Xia, Dinggang Shen, Chunfeng Lian, Li Wang, Hannah H. Deng, Steve H. Fung, Dong Nie, Kim-Han Thung, Pew-Thian Yap, and Jaime Gateno. One-shot generative adversarial learning for MRI segmentation of craniomaxillofacial bony structures. *IEEE Trans. Medical Imaging*, 39(3):787–796, 2020.
- [7] Shen Cheng, Yuzhi Wang, Haibin Huang, Donghao Liu, Haoqiang Fan, and Shuaicheng Liu. Nbnnet: Noise basis learning for image denoising with subspace projection. In *CVPR*, 2021.
- [8] Lu Chi, Borui Jiang, and Yadong Mu. Fast fourier convolution. In Hugo Larochelle, Marc'Aurelio Ranzato, Raia Hadsell, Maria-Florina Balcan, and Hsuan-Tien Lin, editors, *NeurIPS*, 2020.
- [9] Lu Chi, Guiyu Tian, Yadong Mu, Lingxi Xie, and Qi Tian. Fast non-local neural networks with spectral residual learning. In *ACM MM*, 2019.
- [10] Sung-Jin Cho, Seo-Won Ji, Jun-Pyo Hong, Seung-Won Jung, and Sung-Jea Ko. Rethinking coarse-to-fine approach in single image deblurring. In *ICCV*, 2021.
- [11] Chao Dong, Chen Change Loy, Kaiming He, and Xiaoou Tang. Image super-resolution using deep convolutional networks. *IEEE Trans. Pattern Anal. Mach. Intell.*, 38(2):295–307, 2016.
- [12] Hongyun Gao, Xin Tao, Xiaoyong Shen, and Jiaya Jia. Dynamic scene deblurring with parameter selective sharing and nested skip connections. In *CVPR*, 2019.
- [13] Yong Guo, Jian Chen, Jingdong Wang, Qi Chen, Jie Zhang Cao, Zeshuai Deng, Yanwu Xu, and Mingkui Tan. Closed-loop matters: Dual regression networks for single image super-resolution. In *CVPR*, 2020.
- [14] Kaiming He, Xiangyu Zhang, Shaoqing Ren, and Jian Sun. Deep residual learning for image recognition. In *CVPR*, 2016.
- [15] Zhe Hu, Sunghyun Cho, Jue Wang, and Ming-Hsuan Yang. Deblurring low-light images with light streaks. In *CVPR*, 2014.
- [16] Kui Jiang, Zhongyuan Wang, Peng Yi, Chen Chen, Baojin Huang, Yimin Luo, Jiayi Ma, and Junjun Jiang. Multi-scale progressive fusion network for single image deraining. In *CVPR*, 2020.
- [17] Ali Karaali and Cláudio R. Jung. Edge-based defocus blur estimation with adaptive scale selection. *IEEE Trans. Image Process.*, 27(3):1126–1137, 2018.
- [18] Diederik P. Kingma and Jimmy Ba. Adam: A method for stochastic optimization. In Yoshua Bengio and Yann LeCun, editors, *ICLR*, 2015.
- [19] Orest Kupyn, Volodymyr Budzan, Mykola Mykhailych, Dmytro Mishkin, and Jiri Matas. Deblurgan: Blind motion deblurring using conditional adversarial networks. In *CVPR*, 2018.
- [20] Orest Kupyn, Tetiana Martyniuk, Junru Wu, and Zhangyang Wang. Deblurgan-v2: Deblurring (orders-of-magnitude) faster and better. In *ICCV*, 2019.
- [21] Junyong Lee, Sungkil Lee, Sunghyun Cho, and Seungyong Lee. Deep defocus map estimation using domain adaptation. In *CVPR*, 2019.
- [22] Junyong Lee, Hyeongseok Son, Jaesung Rim, Sunghyun Cho, and Seungyong Lee. Iterative filter adaptive network for single image defocus deblurring. In *CVPR*, 2021.
- [23] Jingyun Liang, Jie Zhang Cao, Guolei Sun, Kai Zhang, Luc Van Gool, and Radu Timofte. Swinir: Image restoration using swin transformer. In *ICCV Workshop*, 2021.
- [24] Bee Lim, Sanghyun Son, Heewon Kim, Seungjun Nah, and Kyoung Mu Lee. Enhanced deep residual networks for single image super-resolution. In *CVPR Workshops*, 2017.
- [25] Ilya Loshchilov and Frank Hutter. SGDR: stochastic gradient descent with warm restarts. In *ICLR*, 2017.
- [26] Yiqun Mei, Yuchen Fan, and Yuqian Zhou. Image super-resolution with non-local sparse attention. In *CVPR*, 2021.
- [27] Seungjun Nah, Tae Hyun Kim, and Kyoung Mu Lee. Deep multi-scale convolutional neural network for dynamic scene deblurring. In *CVPR*, 2017.
- [28] Jin-shan Pan, Deqing Sun, Hanspeter Pfister, and Ming-Hsuan Yang. Blind image deblurring using dark channel prior. In *CVPR*, 2016.
- [29] Dongwon Park, Dong Un Kang, Jisoo Kim, and Se Young Chun. Multi-temporal recurrent neural networks for progressive non-uniform single image deblurring with incremental temporal training. In *ECCV*, 2020.
- [30] Kuldeep Purohit and A. N. Rajagopalan. Region-adaptive dense network for efficient motion deblurring. In *AAAI*, 2020.
- [31] Yongming Rao, Wenliang Zhao, Zheng Zhu, Jiwen Lu, and Jie Zhou. Global filter networks for image classification. In *NeurIPS*, 2021.
- [32] Dongwei Ren, Kai Zhang, Qilong Wang, Qinghua Hu, and Wangmeng Zuo. Neural blind deconvolution using deep priors. In *CVPR*, 2020.
- [33] Jaesung Rim, Haeyun Lee, Jucheol Won, and Sunghyun Cho. Real-world blur dataset for learning and benchmarking deblurring algorithms. In Andrea Vedaldi, Horst Bischof, Thomas Brox, and Jan-Michael Frahm, editors, *ECCV*, 2020.
- [34] Oren Rippel, Jasper Snoek, and Ryan P. Adams. Spectral representations for convolutional neural networks. In *NeurIPS*, 2015.
- [35] Olaf Ronneberger, Philipp Fischer, and Thomas Brox. U-net: Convolutional networks for biomedical image segmentation.

In Nassir Navab, Joachim Hornegger, William M. Wells III, and Alejandro F. Frangi, editors, *MICCAI*, 2015.

[36] Christian J. Schuler, Michael Hirsch, Stefan Harmeling, and Bernhard Schölkopf. Learning to deblur. *IEEE Trans. Pattern Anal. Mach. Intell.*, 38(7):1439–1451, 2016.

[37] Ziyi Shen, Wenguan Wang, Xiankai Lu, Jianbing Shen, Haibin Ling, Tingfa Xu, and Ling Shao. Human-aware motion deblurring. In *ICCV*, 2019.

[38] Jianping Shi, Li Xu, and Jiaya Jia. Just noticeable defocus blur detection and estimation. In *CVPR*, 2015.

[39] Maitreya Suin, Kuldeep Purohit, and A. N. Rajagopalan. Spatially-attentive patch-hierarchical network for adaptive motion deblurring. In *CVPR*, 2020.

[40] Jian Sun, Wenfei Cao, Zongben Xu, and Jean Ponce. Learning a convolutional neural network for non-uniform motion blur removal. In *CVPR*, 2015.

[41] Roman Suvorov, Elizaveta Logacheva, Anton Mashikhin, Anastasia Remizova, Arsenii Ashukha, Aleksei Silvestrov, Naejin Kong, Harshith Goka, Kiwoong Park, and Victor Lempitsky. Resolution-robust large mask inpainting with fourier convolutions. In *WACV*, 2022.

[42] Xin Tao, Hongyun Gao, Xiaoyong Shen, Jue Wang, and Jiaya Jia. Scale-recurrent network for deep image deblurring. In *CVPR*, 2018.

[43] Phong Tran, Anh Tuan Tran, Quynh Phung, and Minh Hoai. Explore image deblurring via encoded blur kernel space. In *CVPR*, 2021.

[44] Haohan Wang, Xindi Wu, Zeyi Huang, and Eric P. Xing. High-frequency component helps explain the generalization of convolutional neural networks. In *CVPR*, 2020.

[45] Li Xu, Shicheng Zheng, and Jiaya Jia. Unnatural L0 sparse representation for natural image deblurring. In *CVPR*, 2013.

[46] Yanchao Yang and Stefano Soatto. FDA: fourier domain adaptation for semantic segmentation. In *CVPR*, 2020.

[47] Yuan Yuan, Wei Su, and Dandan Ma. Efficient dynamic scene deblurring using spatially variant deconvolution network with optical flow guided training. In *CVPR*, 2020.

[48] Syed Waqas Zamir, Aditya Arora, Salman H. Khan, Munawar Hayat, Fahad Shahbaz Khan, Ming-Hsuan Yang, and Ling Shao. Learning enriched features for real image restoration and enhancement. In *ECCV*, 2020.

[49] Syed Waqas Zamir, Aditya Arora, Salman H. Khan, Munawar Hayat, Fahad Shahbaz Khan, Ming-Hsuan Yang, and Ling Shao. Multi-stage progressive image restoration. In *CVPR*, 2021.

[50] Matthew D. Zeiler and Rob Fergus. Visualizing and understanding convolutional networks. In *ECCV*, 2014.

[51] Hongguang Zhang, Yuchao Dai, Hongdong Li, and Piotr Koniusz. Deep stacked hierarchical multi-patch network for image deblurring. In *CVPR*, 2019.

[52] Jiawei Zhang, Jinshan Pan, Jimmy S. J. Ren, Yibing Song, Linchao Bao, Rynson W. H. Lau, and Ming-Hsuan Yang. Dynamic scene deblurring using spatially variant recurrent neural networks. In *CVPR*, 2018.

[53] Kaihao Zhang, Wenhan Luo, Yiran Zhong, Lin Ma, Björn Stenger, Wei Liu, and Hongdong Li. Deblurring by realistic blurring. In *CVPR*, 2020.

[54] Yulun Zhang, Yapeng Tian, Yu Kong, Bineng Zhong, and Yun Fu. Residual dense network for image super-resolution. In *CVPR*, 2018.

[55] Zhisheng Zhong, Tiancheng Shen, Yibo Yang, Zhouchen Lin, and Chao Zhang. Joint sub-bands learning with clique structures for wavelet domain super-resolution. In *NeurIPS*, 2018.

[56] Wenbin Zou, Mingchao Jiang, Yunchen Zhang, Liang Chen, Zhiyong Lu, and Yi Wu. Sdwnet: A straight dilated network with wavelet transformation for image deblurring. In *ICCV Workshop*, 2021.